



# Open-source multi-purpose sensor for measurements in continuous capillary flow

Stefan Höving<sup>1</sup> · Jens Bobers<sup>1</sup> · Norbert Kockmann<sup>1</sup>

Received: 7 October 2021 / Accepted: 28 November 2021 / Published online: 9 December 2021  
© The Author(s) 2021

## Abstract

Limited applicability and scarce availability of analytical equipment for micro- and millifluidic applications, which are of high interest in research and development, complicate process development, control, and monitoring. The low-cost sensor presented in this work is a modular, fast, non-invasive, multi-purpose, and easy to apply solution for detecting phase changes and concentrations of optically absorbing substances in single and multi-phase capillary flow. It aims at generating deeper insight into existing processes in fields of (bio-)chemical and reaction engineering. The scope of this work includes the application of the sensor to residence time measurements in a heat exchanger, a tubular reactor for concentration measurements, a tubular crystallizer for suspension detection, and a pipetting robot for flow automation purposes. In all presented applications either the level of automation has been increased or more information on the investigated system has been gained. Further applications are explained to be realized in the near future.

## Article highlights

- An affordable multipurpose sensor for phase differentiation, concentration measurements, and process automation has been developed and characterized
- The sensor is easily modified and can be applied to various tubular reaction/process units for analytical and automation purposes
- Simple integration into existing process control systems is possible

**Keywords** Multiphase flow · Non-invasive sensor · Online concentration measurement · Process automation · Light dependent resistor · Residence time distribution

## Introduction

In research and development of chemical and process engineering, continuous-flow processes have become more and more popular [1]. Although the flexibility of continuous processes lacks some features compared to batch processes [2], attributes such as product quality [3], throughput, efficiency and safety [4] are typical and unique characteristics of continuous processes. The most basic continuous reactor is a pipe or tubular reactor. Reactants are introduced at the inlet and after a desired hydrodynamic residence time the products can be collected at the outlet. These setups are

especially popular due to their convenience and availability of various configurations of tubes. Introducing bends and curves to tubular reactors effects the centrifugal force and induces secondary flow, which in turn improves mixing [5].

Together with the growing interest in continuous processes, miniaturization and modularization of chemical reactors are on the rise [6]. Their large specific surface enables high mass and heat transfer rates [7], and they play a significant role in process intensification [8, 9]. Particularly effects that cause improved internal mixing accompanied with narrow residence time distributions (RTDs) are systematically made use of to achieve high product uniformity [10, 11].

A specific example of a capillary reactor, which is also frequently used for miniaturized chemical reactors is the capillary Coiled Flow Inverter (CFI). A basic schematic is given in Fig. 1. CFIs are tubular or capillary reactors that have been characterized in different configurations and applications [7, 10, 12, 13]. The coil direction of the tube

✉ Stefan Höving  
Stefan.Hoeving@tu-dortmund.de

<sup>1</sup> Department of Biochemical and Chemical Engineering, Laboratory of Equipment Design, TU Dortmund University, Emil-Figge-Straße 68, 44227 Dortmund, Germany

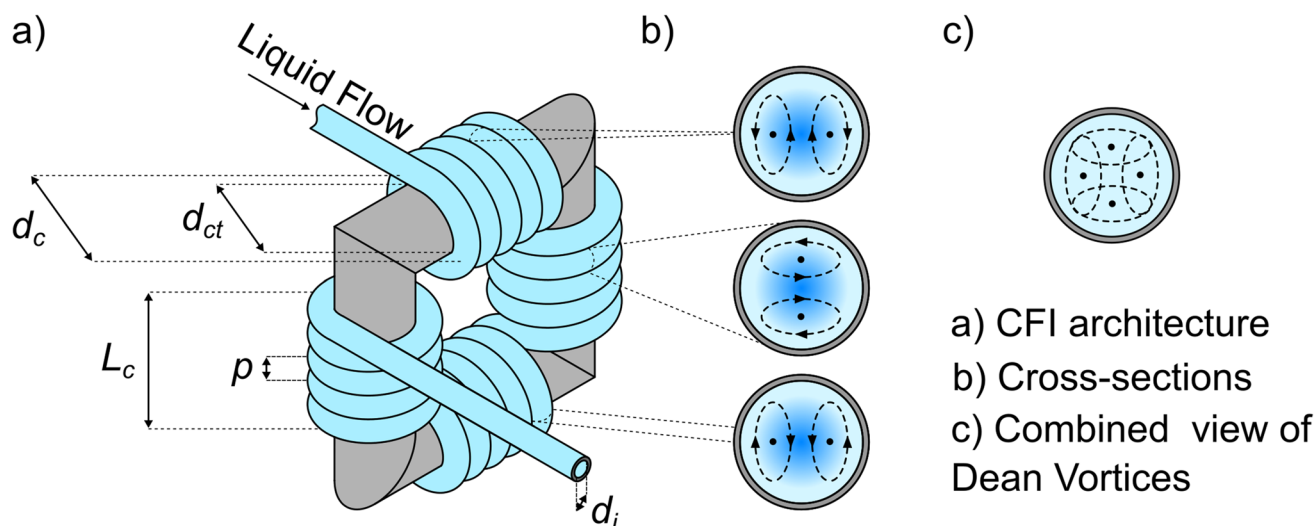


**Fig. 1** **a** Schematic of a Coiled Flow Inverter (CFI). Grey is the supporting structure (frame) for the tube (blue)  $d_c$ : diameter of the frame,  $d_{ct}$ : diameter of coil windings,  $L_c$ : Length of one coil,  $p$ : pitch distance between two turns,  $d_i$ : inner diameter of the tube. **b** Cross-sections

tion of three different positions in the CFI. The blue color gradient is the velocity profile of the fluid inside the tube. Dashed lines describe the circulation of Dean Vortices. **c** Summed up the circulation of Dean Vortices along the tube coordinate

is changed by  $90^\circ$  after a certain amount of turns. The coils cause centrifugal forces on the fluid elements, resulting in secondary flow (Dean flow) and therefore in increased mixing and a narrow residence time distribution in single phase flow [14]. When it comes to two-phase flow within the slug flow regime, secondary Taylor vortices are also induced due to the interfacial boundary of the phases. This provides for internal convection and enhanced interfacial diffusion between contacting fluid compartments (slugs) [15–17]. More precise CFI design guidelines can be found in [18].

Considering a two-phase liquid/liquid system in a tubular reactor, two slugs of the discontinuous phase can be seen as individual reaction compartments that do not directly interact with each other due to spatial separation. For microfluidic applications this has already been used in droplet-based high-throughput screening systems for chemical analysis such as described in [19].

The analysis of the phase of interest is often done with offline methods for which a phase separation is necessary. However, when the flow regime should not be disturbed, phase separators and invasive analytical devices are not eligible. This also holds for most commercially available UV–Vis spectrometers that disturb the flow regime due to changes in the cross sectional area of the flow cell. Noninvasive and online analysis of the individual reaction compartments is often done with camera setups observing the phases in optically accessible tubing [20]. Non-invasive methods include, next to the mentioned optical ones, also acoustical ones. Contributions reporting the quantification of phase proportions, velocities and contents can be found [21–24]. However, flexible, non-invasive and reasonably

priced sensors capable of phase detection and quantitative analysis in micro- and millifluidic applications are often limited to unwieldy camera [20, 25] and ultrasonic setups [20], that do not always fit into small-scale and laboratory setups.

Minimal invasive conductive sensors for detecting phases are described in [24], measuring changes in electrical resistance of the fluids of interest. A capacitive, and therefore non-invasive, solution is presented in [22] and used to differentiate between oil and water in a tubular flow. By measuring the impedance instead of the fluid's resistance, it has been shown that non-invasive measurement of conductivity is possible to distinguish between different phases, too [23]. In a recent contribution, *von Vietinghoff et al.* presented a multi-transistor sensor used to determine slug flow parameters of a triphasic slug flow of 1-hexanol, water, and nitrogen [21]. The determination of multi-phase flow parameters has been demonstrated for microfluidic tubular reactor setups. *Glötz and Kappe* constructed an open-source photometer and demonstrated applications in flow chemistry [26]. The working principle is similar to the sensor concept presented in this work and used for reactor characterization and the determination of reaction kinetics. It uses optical fibers to connect emitter and detector of the sensor to the region of interest within the tubular experimental setup. This enables for good separation of the reactor from the sensors electric components, which is of interest for applications in explosion-risk areas. Additionally, heat dissipation from the LED to the tube containing the liquid medium is prevented. The setup presented here omits the optical fibers, electrical amplifiers and filters making the whole setup less complex and easier to

understand and apply for the non-specialist. The 3D-printed housing makes it possible to clamp the sensor to a desired position of the used tube instead of having to uninstall the tubing and threading the tube through the sensor.

Additionally, the sensor concept with the printed housing allows for rapid modifications in the design to fit specific needs that goes beyond a straight capillary used for the determination of reactor kinetics and reaction kinetics.

The sensor presented in this work can be applied to different tubular setups due to its non-invasive and optical characteristics. The working principle is known for many years [27] and is based on the optical absorption to infer from the attenuation of light to the composition of a sample. The sensor discussed here represents a flexible application technique of the mentioned principle. The use cases in this contribution describe tubular/capillary applications of an optical non-invasive sensor, demonstrating the flexibility and versatility in four different applications. The working principle as well as details of the developed sensor are described for each application. Together with the conclusion of this work an outlook on further application is given with relevant development opportunities.

## Materials and methods

This chapter starts with a recap of the Lambert–Beer Law and continues with the construction and operation of the developed sensor.

### Lambert–Beer law

The Lambert–Beer Law (Eq. 1) links the radiation intensity of an emitter  $I_0$  passing through a sample ( $I$ ) with the concentration  $c$ , the extinction coefficient  $\epsilon$ , and the thickness  $e$  to the absorbance  $A$ .

$$A \sim E = \log\left(\frac{I_0}{I}\right) = \epsilon c e \quad (1)$$

The application of Lambert–Beer Law comes with several limitations that have to be met to fulfill validity. This includes that the medium of interest must not scatter, e.g. must not be turbid. Furthermore, the concentrations of solved substances have to stay moderately low because the coefficient of absorption becomes dependent on the concentration for high concentrations and a linearity is not given anymore. [28, 29]

### Sensor details

The central piece of the sensor is a light-emitting diode (LED) (peak at 620–640 nm, Tru Components, Germany)

with 5 mm diameter as emitter and light depending resistor (LDR) (NSL-19M51; Luna Innovations Inc., Virginia, United States) as detector with a detection optimum at 550 nm. For the presented use cases a red LED showed the highest sensitivity, but can be easily substituted by other colors (wavelengths) depending on the application. Here the optical properties of the tubing material has to be kept in mind. A comparison of different LEDs can be found in SI10. LDRs contain a photosensitive semiconductor element with a CdS resistor that changes its electrical resistance depending on the light reaching the element. Thus, the intensity of the light reaching the detector can be correlated to the electrical resistance of the LDR. To be able to gain insights on the contents of a tube or capillary, LED and LDR are positioned opposite of each other with the tube between them. To shield the sensor from light from the outside, two different sensor housing versions have been designed and implemented. The larger version fits on tubes with an outer diameter of 3.2 mm, hereafter called Version A. The smaller version fits to tubes with an outer diameter of 1.6 mm, hereafter called Version B (cf. Fig. 2). Besides differences in the tube diameter, the versions differ in shape, which resemble two different approaches to prevent stray light from the outside. Both approaches are the result of iterative preliminary experiments investigating the influence of outside light on the sensor signal. A systematic investigation concerning the design approaches was therefore not carried out. Version A has elongated ends that help preventing light from the outside reaching the detector of the sensor. Version B has two 90° bends forming an S-shape to impede the path of the ambient light. Both versions consist of two 3D-printed housing parts (Black PLA, BASF SE, Germany, printed on Ultimaker S5 (Ultimaker, Utrecht, Netherlands) with 0.1 mm layer height and 40 % infill) that can be manually clamped together. Resource files of technical drawings and CAD-files for both versions can be found in SI2–SI7 of the [Supporting Information](#). Modifying these parts is easy and can be done iteratively with appropriate software to fulfill specific needs. LDR and LED are fixed in the designated holes inside the housing parts using molten polylactic acid (PLA). This way, electrical connectors are still accessible from the outside of the housing, while both compartments are protected from light. After fixing the sensor around a tube, LDR and LED face each other with the tube right between them (cf. Fig. 2). This way, the non-invasive working principle can be ensured.

Due to their optical properties tubes made from fluorinated ethylene propylene (FEP) (Bohlender GmbH, Germany), have been selected. FEP is optically transparent and has nearly the same refractive index as water (1.333; depending on the temperature) [15], allowing for an optical analysis of the contents.

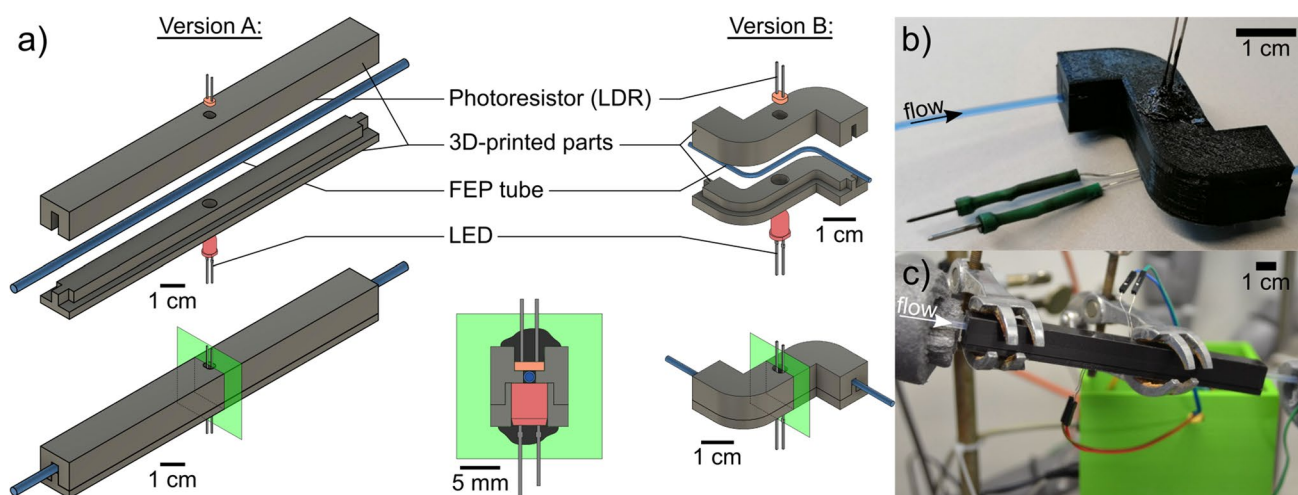


**Fig. 2** **a** Schematic setup of the two sensor versions and cross-section. **b** Photograph of the s-shaped sensor clamped to a FEP tube (1.6 mm o.d., 1 mm i.d.). The tube is filled with diluted dye. **c** Photograph of the straight sensor clamped to a FEP tube (3.2 mm o.d., 1.6 mm i.d.)

### Software and electric circuit

As it has been mentioned before, the electrical components of the sensor are LED and LDR. To make processing and easy interfacing possible, a microcontroller has been selected with the Arduino UNO (Arduino S.r.l., Monza, Italy). As it can be seen in Fig. 3b), the LED, providing the light, is powered with 5 V from a digital pin (2) of the Arduino. A variable resistor or potentiometer connected in series with the LED can be used to adjust the intensity of the emitted light. An LED with a forward voltage of 2.1 V in series with resistors of more than 220  $\Omega$  would consume < 30 mW. A need for active cooling was not observed. The LDR is connected from the 5 V pin to an analog input pin of the Arduino. A 10 k $\Omega$  pull-down-resistor is connected

to ground. This way, the LDRs resistance can be measured as an analog signal by the microcontroller. The resistance of the LDR correlates with the incoming light. The Arduino contains a 10-bit analog to digital converter. This means that the analog resistance (or signal) is mapped to integer values from 0 to 1023. This resolution did not pose challenges in the conducted experiments. If a higher resolution was necessary, different platforms or expansion boards could be used.

The program (cf. Fig. 3a)) installed on the Arduino is written in C++ running on the Arduino IDE (integrated development environment). A minimum working example (MWE) is provided in Fig. 3a) and in SI8. A more complex code for two sensors is provided in SI9. For the operation only 8 lines of code are necessary. In the *setup()* the LED is turned on and a serial connection to a serial host with a

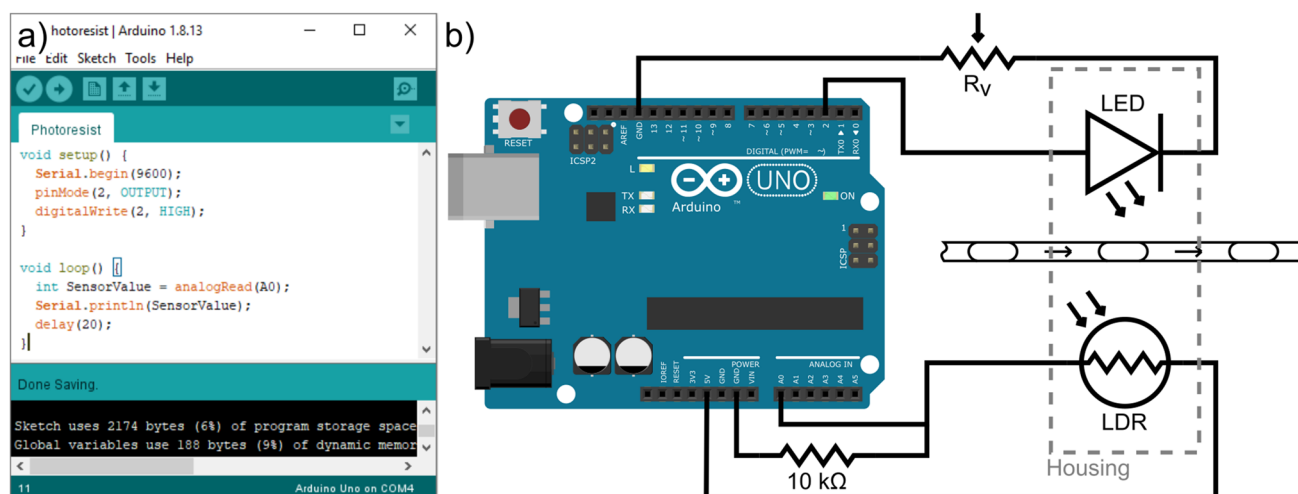


**Fig. 3** **a** Screenshot of the Arduino IDE with a minimum working example code used to run the sensor. **b** Simplified electronic wiring diagram of the Arduino and sensor. This setup can be operated with the program in **a**)

baud rate of 9600 is established. Inside the *loop()*, the analog value obtained from the LDR is saved to the *SensorValue* variable, which is repeatedly printed via the serial connection. A delay of 20 ms is inserted within the *loop()*. This time scale is a compromise between the performance of the Arduino and measurement resolution as well as amount of generated data. With this code, a measuring frequency of 50 Hz is achieved which did not pose challenges regarding data lag due to the faster serial connection. The use of the *millis()* function would make the timing more efficient, while increasing the program's complexity. For reasons of simplicity, the *delay()* function is used here.

The data is provided via the serial port of the Arduino, from where it can be accessed by a serial host. Depending on the platform, the data can be directly integrated into an application, or a simple program can be written that allows for access to the data. The serial interface ensures maximum flexibility. In our use case, it was implemented into different systems such as a custom written process automation system installed on a computer [25] and the process automation software LabVision® (HiTec Zang GmbH, Germany).

## Results from use cases

In this section four different use cases that have been investigated are presented. Qualitative analysis for the sake of automation but also quantitative analysis has been performed in different tubular experimental setups. The capability to distinguish between phases in multi-phase setups, determine the concentration of certain substances in a solution and associated opportunities for process automation will be presented.

### Use case 1: Residence time distribution in micro- and milli-fluidic elements

The residence time of a process fluid in an equipment of interest is an important design parameter. As mentioned before, narrow residence time distributions (RTD) can positively impact the process, such as favoring the main product of a chemical reaction. Considering a tubular reactor with laminar flow accompanied by secondary flow, high radial mixing -from secondary flow- and low axial dispersion lead to narrow residence time distributions. Commonly residence time distributions are determined with sensors that measure the electrical resistance of the fluid to track a highly conductive tracer solution as in [30]. Furthermore, tracking the absorption of a tracer with a commercially available analytical optical device such as an UV-/Vis is possible [31]. However, the installation of an UV-/Vis-spectrometer in a process is not always possible for reasons of available space. The same holds for conductivity sensors that even have to be

installed invasively. Therefore, the developed sensor is used to track the concentration of an optically visible tracer solution to have insights on the RTD of milli-fluidic elements in a non-invasive manner by simply clamping the sensor to the existing FEP tubing of the fluidic element.

From the recorded raw data the RTD function of the heat exchanger at the outlet  $E(t)$  and the cumulative function  $F(\tau)$  have been calculated according to [32]. Applying the axial dispersion model and a curve fitting method characteristic values such as the axial dispersion coefficient ( $D_{ax}$ ) and consequently the Bodenstein number ( $Bo$ ) can be determined [32]. The fluidic element considered in this use case is a heat exchanger passage with one inlet and one outlet for heat exchanger medium flow. Inlet and outlet of the heat exchanger are connected to an FEP tube (3.2 mm o.d., 1.6 mm i.d.). Further specifications and details of the heat exchanger are beyond the scope of this work. The heat exchanger will therefore be treated as a black-box. Two sensors (Version A) are clamped to the tubes, one directly at the outlet, and one directly at the inlet (edge to edge). Deionized water was pumped ( $320.3 \text{ mL min}^{-1}$ ) through the heat exchanger with a gear pump (Ismatec®ISM446B; Cole-Parmer GmbH, Wertheim, Germany) as process medium. Through a septum, water soluble tracer solution (0.15 mL black ink (Metzger & Mendle GmbH, Fischach, Germany)) was quickly ( $\ll 1 \text{ s}$ ) injected by hand into the process medium stream right before the first sensor using a syringe (schematic in Fig. 4). This does influence the flowrate during the injection. The effect of this on the RTD however should be negligible. Both sensor signals were recorded over time (Fig. 4).

From Fig. 4 a narrow peak is visible that resembles the signal measured at the inlet of the heat exchanger (blue). The tracer travels through the heat exchanger and exits at the outlet, where sensor 2 recorded the output signal (brown). As one can see from the signals the tracer enters the fluidic element with a narrow pseudo-Dirac delta function (unit impulse), experiences axial mixing, and exits with a substantially broader RTD.

### Use case 2: Enzymatic gas–liquid reactions

Biocatalytic reactions are of high interest in industry and research. This is mainly due to the enantio-selective properties of enzymes and the mild reaction conditions in an aqueous environment [20, 25]. A significant role in the respecting reactor systems plays the mass transport of the substrate to the enzyme's active site. Therefore, investigations of different mixing strategies and their influence on mass transport are performed with various approaches [6]. One specific approach makes use of two-phase flow induced vortices in capillary flow [25]. The setup used for the presented data is already introduced in [20]. Here, the

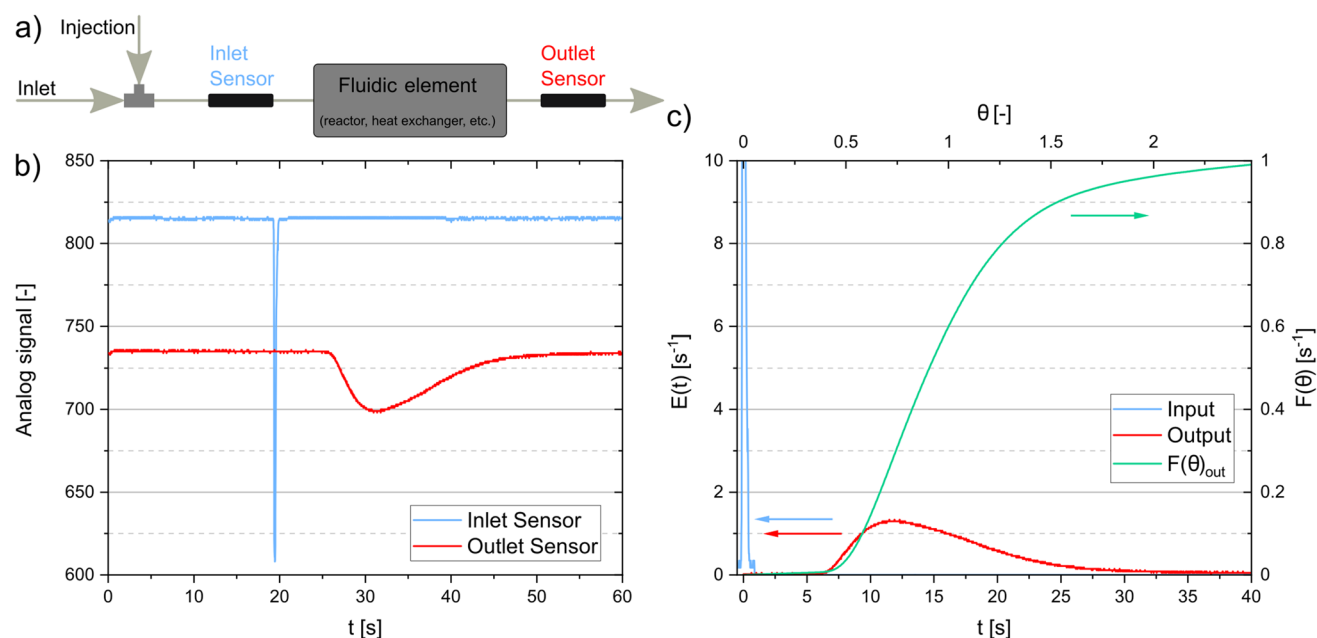


**Fig. 4** a Schematic of heat exchanger and sensor setup. b Analog and unprocessed sensor signal from the Inlet and Outlet Sensor. c Residence time distribution (RTD) of a heat exchanger measured with the

presented sensor by tracking the intensity of injected dye. Input curve is not completely shown

kinetics of the enzymatic oxidation of 2,2'-azino-bis(3-ethylbenzothiazoline-6-sulfonic acid) (ABTS) (Sigma Aldrich, Missouri, USA) is investigated. The catalyzing enzyme used is laccase (Sigma Aldrich, Missouri, USA). This reaction system is frequently used as a model reaction because of the availability of all reactants but even more due to the striking change in color from colorless (ABTS) to blue/green (ABTS<sub>ox</sub>). The chemical analysis here is done in an optical and non-invasive system with a dedicated photography setup [20]. Offline techniques would require significant interventions to the system with quenching procedure to stop enzyme activity would also be necessary in many cases [20, 25]. As an alternative analytic procedure, the optical sensor (version A) discussed here was integrated into the tubular reaction system. The sensor gives insights into the concentration of ABTS<sub>ox</sub> inside the two-phase reaction system. Figure 5 shows the results of a single-phase calibration procedure done with different concentrations of ABTS and different light intensities that are varied using different resistors for  $R_v$  (cf. Fig. 3b)) to later investigate the two-phase system. Therefore, the different concentrations of ABTS in deionized water have been prepared and oxidized using synthetic air until full conversion can be assumed. The prepared solution was continuously pumped ( $9.7 \text{ mL min}^{-1}$ ) through an FEP tube (3.2 mm o.d., and 1.6 mm i.d.) to which the sensor was clamped. To pump the fluid a peristaltic pump (ISM597, Ismatec®, Cole Palmer GmbH, Wertheim, Germany) was used. Data points are achieved

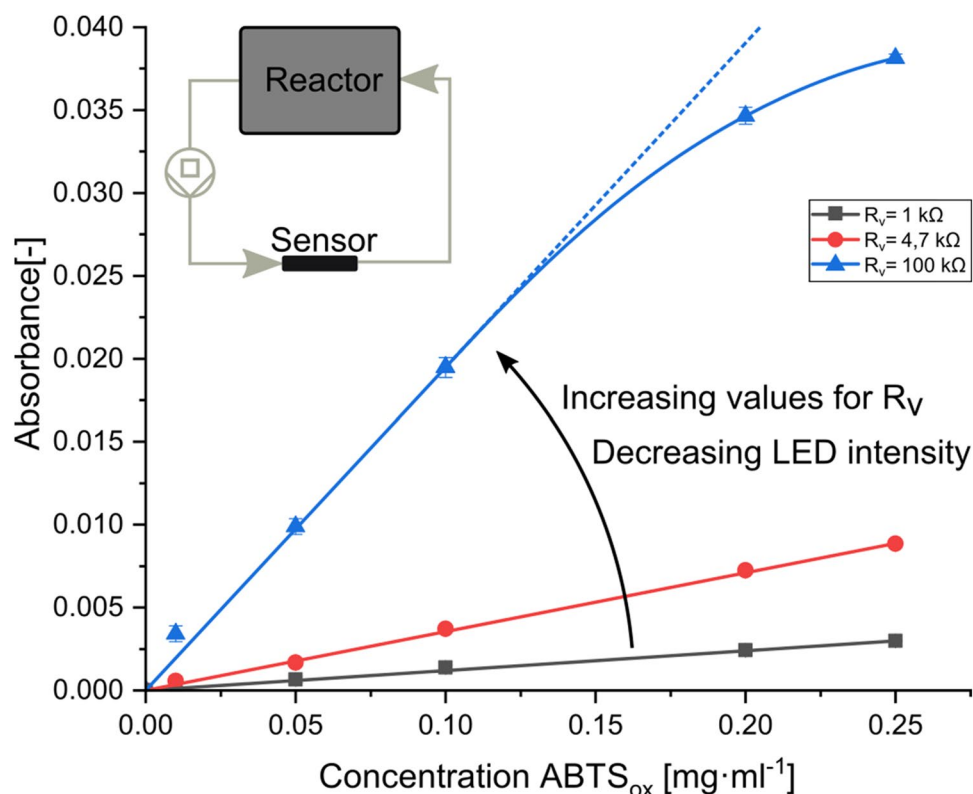
from triple measurements. The absorbance was calculated from the sensors analog signal using Lambert-Beers Law (Eq. 1).

The experimental data show a linear dependency of the concentration and the absorption, as it is required for Lambert-Beer to be applied [27]. By changing the resistance  $R_v$  it is possible to change the sensor's sensitivity, too, which is resembled by the slope of the calibration lines in Fig. 4. The blue curve shows deviation from a straight line (dotted). A linear dependency for concentrations larger than  $0.1 \text{ mg mL}^{-1}$  cannot be observed for  $R_v = 100 \text{ k}\Omega$ . However, for concentrations below  $0.1 \text{ mg mL}^{-1}$  the sensitivity of the calibration curve is better compared to the samples evaluated with smaller values for  $R_v$ , which show a linear dependency across the whole measuring range.

It was possible to show that the sensor can be calibrated to concentrations of ABTS<sub>ox</sub>, which opens up a new method for mass transport investigations in tubular reaction systems such as in [20, 25]. Furthermore, it was demonstrated that the sensitivity of the sensor is strongly dependent on the intensity of the emitter which was varied by systematically changing  $R_v$ . A suitable tradeoff between sensitivity and linear dependency can be found in order to identify an operating window.

This can be of particular interest when using new substance systems because instead of having to decrease the concentration of a substance of interest by dilution, one can simply decrease the intensity of the emitter to reach the linear range of the calibration curve. This could even easily

**Fig. 5** Calibration curves for different concentrations of  $\text{ABTS}_{\text{ox}}$  and different values for  $R_V$ . The absorbance has been calculated with Lambert-Beers law



be integrated into an automation system that checks if the collected data agrees with the conditions to apply the Lambert–Beer Law.

### Use case 3: Suspension detection for continuous crystallization

Research interest in continuous (tubular) crystallizers is increasing, especially in the chemical and pharmaceutical field due to product quality consistency and overall efficiency. Examples for these crystallizers are [33, 34], while they can also have a CFI design [35, 36]. As reported, the generation of solids inside a continuously operated tube is prone to blocking [33, 36, 37]. Clogging can occur due to agglomeration of the solids and growth of crystals on walls, invasive sensors, and valves that act as mechanical hurdles or thermal bridges to the outside. Therefore, flushing and cleaning of the tubular reactors is necessary to maintain the functionality of the device. Since the demand for continuous automated processes is high, an automated cleaning cycle needs to be integrated into the experimental setup. However, rinsing the reactor with solution or even solvent influences the product exiting the crystallizer. A possible dilution in the product vessel or subsequent process steps might even lead to the dissolution of product crystals.

In this use case a continuous tubular crystallizer with a twin stack CFI design is used (cf. Fig. 6). Process medium is

pumped (LabDos easy-load, HiTec Zang GmbH, Germany) through an FEP tube (3.2 mm o.d., 1.6 mm i.d.). In a tube-in-tube setup cooling medium is pumped (CC304, Huber Kältemaschinenbau AG, Germany) through a bigger tube in a counter current fashion to be able to control the temperature along the axial coordinate of the crystallizer. As a model system used for characterization experiments the substance system *L*-alanine/water has been used. Further information on the crystallizer can be found in [38] and [31].

To prevent the washing liquid from being collected together with the product suspension and possibly affecting the product properties, the described sensor was integrated. It was installed at the end of the CFI, 0.5 m from the outlet, before the valve that switches between filling the process medium into the product container and filling it into the waste container. Due to the open-source electronics, it was possible to integrate the Arduino, operating the sensor version A, into the process control system (PCS) LabManager® (HiTec Zang GmbH, Germany), where a logic coupling between the sensors signal and the valve position was implemented.

Figure 6b shows the sensor signal plotted over time for a crystallization process with two cleaning cycles (10–13 min, 18–22 min). The images taken with microscope (Bresser Science ADL 601P, Bresser GmbH, Rhede, Germany) and an attached camera (Z6, Nikon GmbH, Tokyo, Japan) show

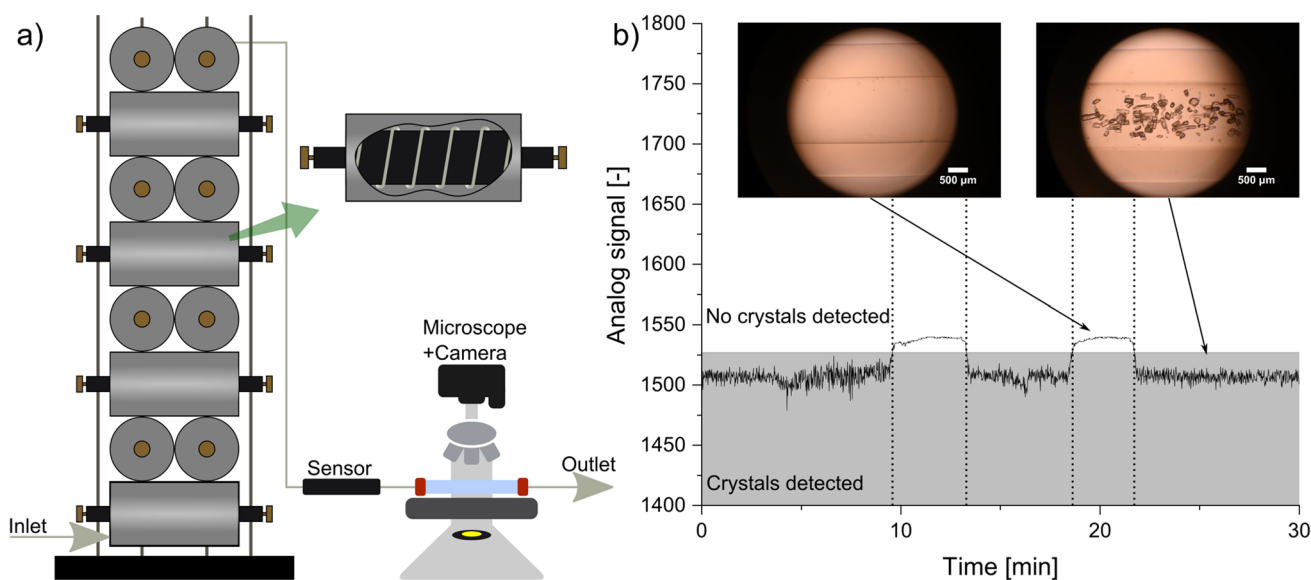


**Fig. 6** a Schematic setup of the CFI crystallizer with a camera setup at the suspension outlet. The sensor (version A) installed close to the microscope delivers the analog signal shown in b). Here the grey box

depicts the static threshold used for the evaluation of crystal presence. The images are exemplary for both states

both states, crystal suspension and solvent. As one can see, the sensor signal changes significantly depending on the prevailing state enabling the usage of the signal as a trigger for the valve position.

Utilizing this information and the subsequent signal processing of the PCS as well as a suitable valve positioning strategy, it was possible to separate the solvent for purging from the product suspension stream in order to increase the overall product quality and process performance.

#### Use case 4: Automation of continuous liquid–liquid reaction systems

Lab automation has become more and more prominent in recent years [39, 40]. It opens up potentials concerning decreasing manual and tedious work while maintaining and increasing reproducibility and significance of experimental results [41]. Especially for batch screenings pipetting robots have shown to be a reliable although financially expensive way to handle liquid dosing operations [39, 41]. According to this trend, an automated dosage system (ADoS) has been developed in our research group to increase the throughput of chemical batch reactions [42].

As a step toward automated continuous processes, a tubular reactor in form of a CFI (cf. Fig. 7) bottom right) has been coupled to the pipetting robot (cf. Fig. 7a)). The reactor consists of 4 coils with 15 turns of FEP tubing (1.6 mm o.d., 1 mm i.d.). Each coil consists of 1 m tube. More specific information on the reactor configuration can be found in [25]. A continuous phase is pumped through a droplet

injection unit (cf. Fig. 7a) bottom left) into the CFI with flow rates in the range of  $40 \mu\text{L min}^{-1}$  to  $3 \text{ mL min}^{-1}$  by a syringe pump (LAMBDA VIT-FIT, LAMBDA Instruments GmbH, Baar, Switzerland). For validation experiments a continuous phase of colored ( $0.25 \text{ mg mL}^{-1}$  Sudan Blue II (Sigma Aldrich, St. Louis, Missouri, USA)) polydimethylsiloxane (PDMS) (ELBESIL-Öle, B. L. Böwing GmbH, Hofheim, Germany, 1 cSt,  $945 \text{ kg}\cdot\text{m}^{-3}$ ) and a disperse phase of deionized water were used. Using the injection unit, the ADoS is capable of injecting water slugs of desired volume into the continuous phase. Figure 7d) shows the signal of water slugs of different volume that have been recorded by sensor 2 (Version B) which is positioned at the outlet of the CFI (cf. Fig. 7a)). The flowrate during the measurement was set to  $63.12 \mu\text{L min}^{-1}$ . Figure 7d) shows photographs of the same slugs also taken after they had passed the reactor.

It was not only possible to distinguish the continuous from the disperse phase, from the signal it may also be possible to use the sensor in applications where determining the length of a slug is of interest. Additionally, aqueous slugs with different concentrations of  $\text{ABTS}_{\text{ox}}$  have been injected into the system following the same procedure as described before (cf. Fig. 7b)). Here the PDMS has not been colored blue. It can be seen that the concentration of  $\text{ABTS}_{\text{ox}}$  inside the slugs causes different signals of the sensor, which makes a correlation between both possible.

Low flow rates generate high residence times, however, good mixing within the slugs can only be achieved with high flow rates causing short residence times in the CFI. For reactions that should be screened for a longer time than the



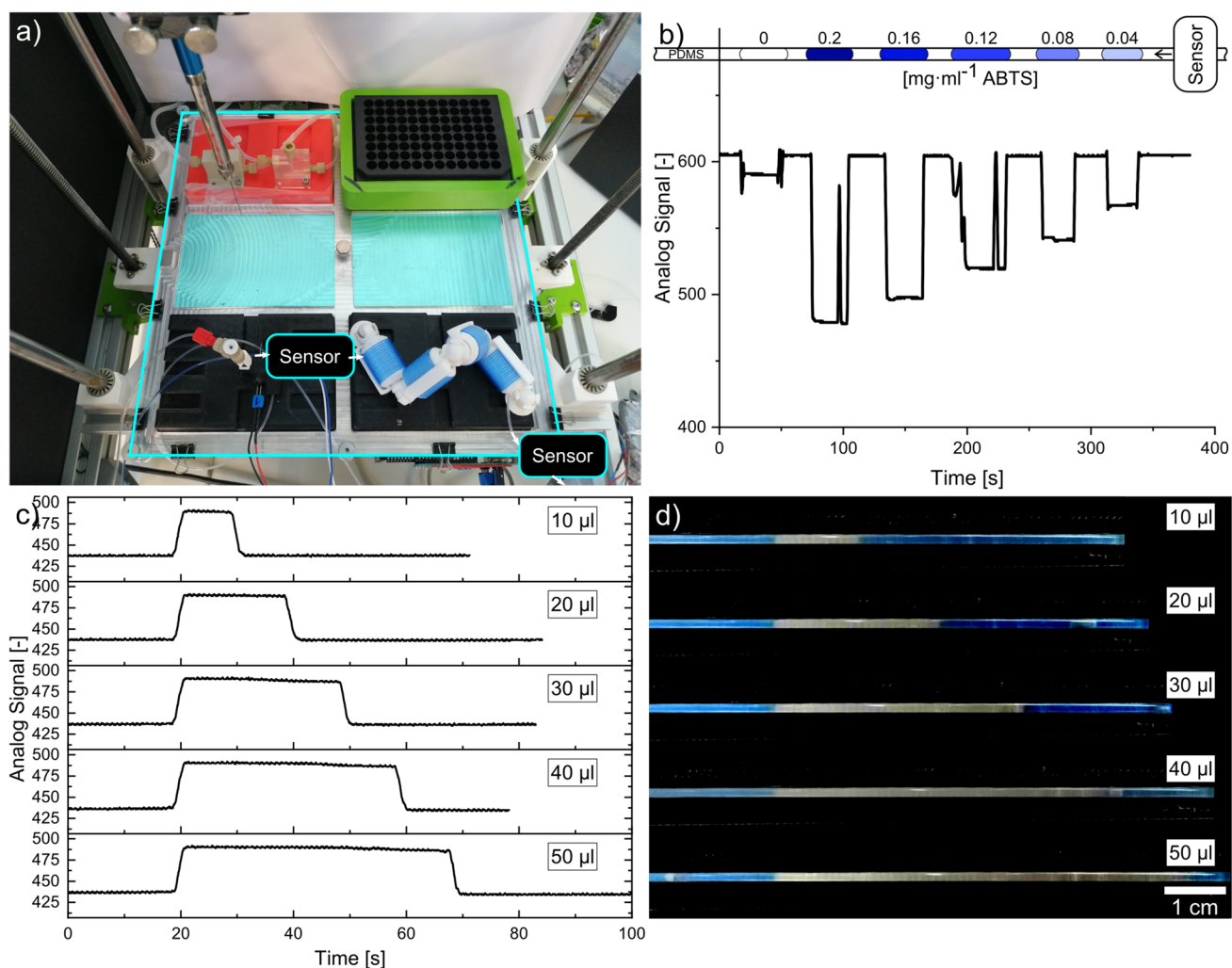


**Fig. 7** **a** Continuous CFI setup inside a pipetting robot with automated dosing system ADoS. Sensor positions for concentration measurements and changing the pump direction are highlighted. **b** Sensor

signal for aqueous  $\text{ABTS}_{\text{ox}}$  slugs of different concentrations with PDMS as continuous phase. **c** Signal for aqueous slugs of different volume in colored PDMS. **d** Images of the slugs shown in **c**

actual residence time the presented CFI reactor can provide for, sensor 1 before and sensor 2 after the reactor come into play. The sensors detect the slugs entering and leaving the reactor and the process automation system automatically changes the pump direction of the syringe pump that is feeding the continuous phase in terms of a feedback. By pumping the slugs back and forth between the two sensors a desired residence time can be achieved.

## Discussion

The presented sensor and its use cases, which resemble an extract of possible applications, has shown to be a viable alternative over traditional analytical equipment. Neither high amounts of data is generated nor complicated processing of such is necessary to operate the sensor or evaluate the

output. In all presented applications the sensor setup was operated by a microcontroller that delivers the output data stream via a standard serial protocol. This enables to simply read the raw data from the controller, while an integration into common automation systems is possible for further control purposes.

The sensor might face limitations when it comes to high concentrations of dissolved analytes due to the nonlinearity of concentration and optical properties in such cases. This is a general issue in optical analysis. The sensor's working principle depends highly on the properties of the materials used. Not only the tubing material needs to be optically accessible but also the fluid of interest needs to be somewhat accessible for (visible) light to be evaluated by the sensor. Here, the sensor was used with FEP-tubes with an outer diameter of 3.2 mm (1.6 mm i.d.) and 1.6 mm (1 mm i.d.), however the sensors geometry is easily modifiable and

should work for different tube sizes or view glass arrangements as well. Tube material and configurations such as wall thickness and opacity can influence the sensor's sensitivity.

In multi-phase systems, where the phases have the same or similar optical properties such as absorption maxima and refractive indices the sensor might reach its limits. The sensor signal may only change in a non-distinctive way and not overcome a certain threshold necessary for distinction. Here it was possible to color one of the phases with an inert dye which helped to overcome this challenge. For fully developed slug flows a discrimination between the two phases was possible this way. However, a qualitative information about complex systems with different phases or concentrations is often valuable for better process understanding.

In this contribution the sensor has been connected to a flexible Arduino UNO microcontroller reading the data with a frequency of up to 50 Hz. For applications that require a faster measurement frequency than 50 Hz it would be possible to exchange the Arduino Uno with a development board that has a faster chipset. Stepping away from the Arduino platform could also have a beneficial impact. Arduinos are developed to be user friendly and functional without focusing performance. Standard functions in the Arduino environment cause an overhead that can be avoided by removing the Arduino bootloader and using the programming language preferred by the chipset manufacturer.

The overall ease of use, flexibility, cost efficiency, and non-invasive character can speed up process development time in different areas. The modular and adaptable design of the multipurpose sensor enables transferring the working principle to applications and problems that are beyond those presented in this contribution. The “clamp-on” feature makes mounting and dismounting to setups that already contain optically accessible tubular compartments especially easy. Emitter and detector of the same form factor are available in different configurations (e.g. emission/ detection spectra and optima) which allows for custom tailored solutions with regard to the optical properties of emitter, detector, and the substance of interest. This way it would be possible to track concentration changes of a reactant along a tube with several sensors installed in series along the length of the tube. It would also be feasible to design the housing of the sensor to fit curved tubes so that measurements could also be performed between the individual coils of a CFI at the 90° bends. Applications are conceivable for electromagnetic waves outside the visible spectrum, too. Another field of application could be the use of the sensor as a tool to classify the product of tubular crystallizers. Here the change of absorbance for different particles can be utilized. With regards to cost, the sensor itself is very affordable with material costs less than 1.5 € per piece (see S11). The microcontroller is not included because it is optional and not limited to one sensor. This

makes it possible to integrate a large number of inline sensors to get more data out of a process. To get relevant information from the data is another step, which has to be tackled with proper data management and analysis tools [43].

## Conclusion & outlook

The presented optical sensor and its working principle for the analysis of capillary single and multi-phase flow phenomena are an interesting choice compared to common analytical methods such as spectrometer and conductivity meter as well as camera setups that generate information from images. Although the working principle of using optical absorption to infer from the attenuation of light to the composition of the sample is known for a long time [27], this contribution presents new aspects regarding laboratory applications. By detecting differences in light absorption of samples or process streams the presented sensor provides reliable online process information with a simple electrical setup. Its capabilities with regards to solid phase detection, process automation, process monitoring for biochemical reactions, and determination of RTD characteristics have been demonstrated in a quantitative or qualitative way.

The installed program making the data accessible is easy to understand for non-professionals and adaptable for specific needs. Further applications would allow for parallelized systems with more than two sensors connected to one microcontroller recoding the intensity of several wavelengths at once, achieving more specific results of a sample. Also, skipping the microcontroller, while connecting the sensor directly to an existing process control system is possible. There is a wide variety of possible applications within the field of flow chemistry. Especially the differentiation of phases, capabilities in automation, and the determination of RTDs of fluidic elements are of high interest. Straightforward software and hardware design enable for the integration of both into already existing processes constituting an attractive possibility to increase process knowledge and automation.

**Supplementary Information** The online version contains supplementary material available at <https://doi.org/10.1007/s41981-021-00214-w>.

**Acknowledgements** This research was partly supported by the AiF foundation (grant no. ZF4595601LL8 for UC1), the German Research Foundation (DFG, grant no. KO2349/13-1 for UC2), and German Ministry of Economic Affairs and Energy BMWi (ENPRO2.0-TeiA, grant no. 03ET1528A). We would like to thank research associates and students that let us implement the sensor into their setups or even implemented them themselves. These include Mira Schmalenberg, Stephanie Kreis, Julia Grünh, Hüseyin Talha Eroglu, Murat Oruç, Daniel Becker, and Jan-Hendrik Seifert.

**Funding** Open Access funding enabled and organized by Projekt DEAL.

## Declarations

**Conflict of interest** The authors have declared no conflict of interest.

**Open Access** This article is licensed under a Creative Commons Attribution 4.0 International License, which permits use, sharing, adaptation, distribution and reproduction in any medium or format, as long as you give appropriate credit to the original author(s) and the source, provide a link to the Creative Commons licence, and indicate if changes were made. The images or other third party material in this article are included in the article's Creative Commons licence, unless indicated otherwise in a credit line to the material. If material is not included in the article's Creative Commons licence and your intended use is not permitted by statutory regulation or exceeds the permitted use, you will need to obtain permission directly from the copyright holder. To view a copy of this licence, visit <http://creativecommons.org/licenses/by/4.0/>.

## References

- Baumann M, Moody TS, Smyth M et al (2020) A perspective on continuous flow chemistry in the pharmaceutical industry. *Org Process Res Dev* 24:1802–1813. <https://doi.org/10.1021/acs.oprd.9b00524>
- Nagy ZK, El Hagrasy A, Litster J (2020) Continuous pharmaceutical processing. Springer, Cham
- Plumb K (2005) Continuous processing in the pharmaceutical industry. *Chem Eng Res Des* 83:730–738. <https://doi.org/10.1205/cherd.04359>
- Grundemann L, Schoenitz M, Scholl S (2012) Shorter time-to-market with micro-conti processes. *Chem Ing Tech* 84:685–693. <https://doi.org/10.1002/cite.201100238>
- Schönfeld F, Hardt S (2004) Simulation of helical flows in microchannels. *AIChE J* 50:771–778. <https://doi.org/10.1002/aic.10071>
- Hessel V, Löwe H, Schönfeld F (2005) Micromixers—a review on passive and active mixing principles. *Chem Eng Sci* 60:2479–2501. <https://doi.org/10.1016/j.ces.2004.11.033>
- Mridha M, Nigam K (2008) Coiled flow inverter as an inline mixer. *Chem Eng Sci* 63:1724–1732. <https://doi.org/10.1016/j.ces.2007.10.028>
- Jähnisch K, Hessel V, Löwe H et al (2004) Chemistry in microstructured reactors. *Angew Chem Int Ed Engl* 43:406–446. <https://doi.org/10.1002/anie.200300577>
- Hessel V, Löwe H (2003) Microchemical engineering: components, plant concepts, user acceptance – part III. *Chem Eng Technol* 26:531–544. <https://doi.org/10.1002/ceat.200390079>
- Kumar V, Mridha M, Gupta AK et al (2007) Coiled flow inverter as a heat exchanger. *Chem Eng Sci* 62:2386–2396. <https://doi.org/10.1016/j.ces.2007.01.032>
- Schmalenberg M, Krieger W, Kockmann N (2019) Modular coiled flow inverter with narrow residence time distribution for process development and production. *Chem Ing Tech* 91:567–575. <https://doi.org/10.1002/cite.201800172>
- Mandal MM, Aggarwal P, Nigam KDP (2011) Liquid-liquid mixing in coiled flow inverter. *Ind Eng Chem Res* 50:13230–13235. <https://doi.org/10.1021/ie2002473>
- Mansour M, Thévenin D, Zähringer K (2020) Numerical study of flow mixing and heat transfer in helical pipes, coiled flow inverters and a novel coiled configuration. *Chem Eng Sci* 221:115690. <https://doi.org/10.1016/j.ces.2020.115690>
- Saxena AK, Nigam KDP (1984) Coiled configuration for flow inversion and its effect on residence time distribution. *AIChE J* 30:363–368. <https://doi.org/10.1002/aic.690300303>
- Sharma L, Nigam K, Roy S (2017) Single phase mixing in coiled tubes and coiled flow inverters in different flow regimes. *Chem Eng Sci* 160:227–235. <https://doi.org/10.1016/j.ces.2016.11.034>
- Kumar V, Aggarwal M, Nigam K (2006) Mixing in curved tubes. *Chem Eng Sci* 61:5742–5753. <https://doi.org/10.1016/j.ces.2006.04.040>
- Castelain C, Berger D, Legentilhomme P et al (2000) Experimental and numerical characterisation of mixing in a steady spatially chaotic flow by means of residence time distribution measurements. *Int J Heat Mass Transfer* 43:3687–3700. [https://doi.org/10.1016/S0017-9310\(99\)00363-4](https://doi.org/10.1016/S0017-9310(99)00363-4)
- Kurt SK, Akhtar M, Nigam KDP et al (2017) Continuous reactive precipitation in a coiled flow inverter: inert particle tracking, modular design, and production of uniform CaCO<sub>3</sub> particles. *Ind Eng Chem Res* 56:11320–11335. <https://doi.org/10.1021/acs.iecr.7b02240>
- Engl W, Tachibana M, Colin A et al (2008) A droplet-based high-throughput tubular platform to extract rate constants of slow chemical reactions. *Chem Eng Sci* 63:1692–1695. <https://doi.org/10.1016/j.ces.2007.11.006>
- Grühn J, Vogel M, Kockmann N (2021) Digital image processing of gas-liquid reactions in coiled capillaries. *Chem Ing Tech* 93:825–829. <https://doi.org/10.1002/cite.202000240>
- Vietinghoff N von, Lungrin W, Schulzke R et al. (2020) Photoelectric sensor for fast and low-priced determination of Bi- and triphasic segmented slug flow parameters. *Sensors* 20. <https://doi.org/10.3390/s20236948>
- Demori M, Ferrari V, Strazza D et al (2010) A capacitive sensor system for the analysis of two-phase flows of oil and conductive water. *Sens Actuators A* 163:172–179. <https://doi.org/10.1016/j.sna.2010.08.018>
- Wang YX, Ji HF, Huang ZY et al (2017) Online measurement of conductivity/permittivity of fluid by a new contactless impedance sensor. *Rev Sci Instrum* 88:55111. <https://doi.org/10.1063/1.4983208>
- Fan S, Yan T (2014) Two-phase air-water slug flow measurement in horizontal pipe using conductance probes and neural network. *Trans Instrum Meas* 63:456–466. <https://doi.org/10.1109/TIM.2013.2280485>
- Bobers J, Grühn J, Höving S et al (2020) Two-phase flow in a coiled flow inverter: process development from batch to continuous flow. *Org Process Res Dev* 24:2094–2104. <https://doi.org/10.1021/acs.oprd.0c00152>
- Glötz G, Kappe CO (2018) Design and construction of an open source-based photometer and its applications in flow chemistry. *React Chem Eng* 3:478–486. <https://doi.org/10.1039/C8RE00070K>
- Perkampus H-H (1986) UV-VIS-Spektroskopie und ihre Anwendungen. Springer, Berlin
- Mayerhöfer TG, Popp J (2019) Beer's law - why absorbance depends (almost) linearly on concentration. *ChemPhysChem* 20:511–515. <https://doi.org/10.1002/cphc.201801073>
- Skoog DA, West DM, Holler FJ (2013) Fundamentals of analytical chemistry, 9th edn. Cengage, Belmont
- Soboll S, Bittorf L, Kockmann N (2018) Axial backmixing and residence time distribution in a miniaturized, stirred-pulsed extraction column. *Chem Eng Technol* 41:134–142. <https://doi.org/10.1002/ceat.201700152>
- Schmalenberg M, Weick LK, Kockmann N (2021) Nucleation in continuous flow cooling sonocrystallization for coiled capillary crystallizers. *J Flow Chem*. <https://doi.org/10.1007/s41981-020-00138-x>

32. Levenspiel O (1999) Chemical reaction engineering, 3rd edn. Wiley, New York
33. Eder RJP, Radl S, Schmitt E et al (2010) Continuously seeded, continuously operated tubular crystallizer for the production of active pharmaceutical ingredients. *Cryst Growth Des* 10:2247–2257. <https://doi.org/10.1021/cg9015788>
34. Besenhard MO, Neugebauer P, Ho C-D et al (2015) Crystal size control in a continuous tubular crystallizer. *Cryst Growth Des* 15:1683–1691. <https://doi.org/10.1021/cg501637m>
35. Hohmann L, Greinert T, Mierka O et al (2018) Analysis of crystal size dispersion effects in a continuous coiled tubular crystallizer: experiments and modeling. *Cryst Growth Des* 18:1459–1473. <https://doi.org/10.1021/acs.cgd.7b01383>
36. Hohmann L, Schmalenberg M, Prasanna M et al (2019) Suspension flow behavior and particle residence time distribution in helical tube devices. *Chem Eng J* 360:1371–1389. <https://doi.org/10.1016/j.cej.2018.10.166>
37. Wang Y, Su M, Bai Y (2020) Mechanism of glycine crystal adhesion and clogging in a continuous tubular crystallizer. *Ind Eng Chem Res* 59:25–33. <https://doi.org/10.1021/acs.iecr.9b05977>
38. Schmalenberg M, Hohmann L, Kockmann N (2018) Miniaturized Tubular Cooling Crystallizer With Solid-Liquid Flow for Process Development. In: Proceedings of the ASME 16th International Conference on Nanochannels, Microchannels and Minichannels 2018: Presented at ASME 2018 16th International Conference on Nanochannels, Microchannels and Minichannels, June 10–13, 2018, Dubrovnik, Croatia. The American Society of Mechanical Engineers, New York
39. Prabhu GRD, Urban PL (2017) The dawn of unmanned analytical laboratories. *Trends Anal Chem* 88:41–52. <https://doi.org/10.1016/j.trac.2016.12.011>
40. Urban PL (2018) Prototyping instruments for the chemical laboratory using inexpensive electronic modules. *Angew Chem Int Ed Engl* 57:11074–11077. <https://doi.org/10.1002/anie.201803878>
41. Kong F, Yuan L, Zheng YF et al (2012) Automatic liquid handling for life science: a critical review of the current state of the art. *J Lab Autom* 17:169–185. <https://doi.org/10.1177/2211068211435302>
42. Bobers J, Škopić MK, Dinter R et al (2020) Design of an automated reagent-dispensing system for reaction screening and validation with DNA-tagged substrates. *ACS Comb Sci* 22:101–108. <https://doi.org/10.1021/acscombsci.9b00207>
43. Wulf C, Beller M, Boenisch T et al (2021) A unified research data infrastructure for catalysis research – challenges and concepts. *ChemCatChem* 13:3223–3236. <https://doi.org/10.1002/cctc.202001974>

**Publisher's note** Springer Nature remains neutral with regard to jurisdictional claims in published maps and institutional affiliations.